π and 4π Josephson Effects Mediated by a Dirac Semimetal—Supplement

UT Dallas Author(s):

Zhi-qiang Bao
Fan Zhang

Citation:

Yu, W., W. Pan, D. L. Medlin, M. A. Rodriguez, et al. 2018. "π and 4π Josephson effects mediated by a Dirac semimetal." Physical Review Letters 120(17): art. 177704, doi:10.1103/PhysRevLett.120.177704

SUPPLEMENTAL MATERIAL

π and 4π Josephson Effects Mediated by a Dirac Semimetal

W. Yu[1], W. Pan[1], D. L. Medlin[2], M. A. Rodriguez[1], S. R. Lee[1], Zhi-qiang Bao[3], and F. Zhang[3]

[1]*Sandia National Laboratories, Albuquerque, New Mexico 87185, USA*

[2]*Sandia National Laboratories, Livermore, CA 94551, USA*

[3]*Department of Physics, University of Texas at Dallas, Dallas, TX, USA*

x-ray diffraction

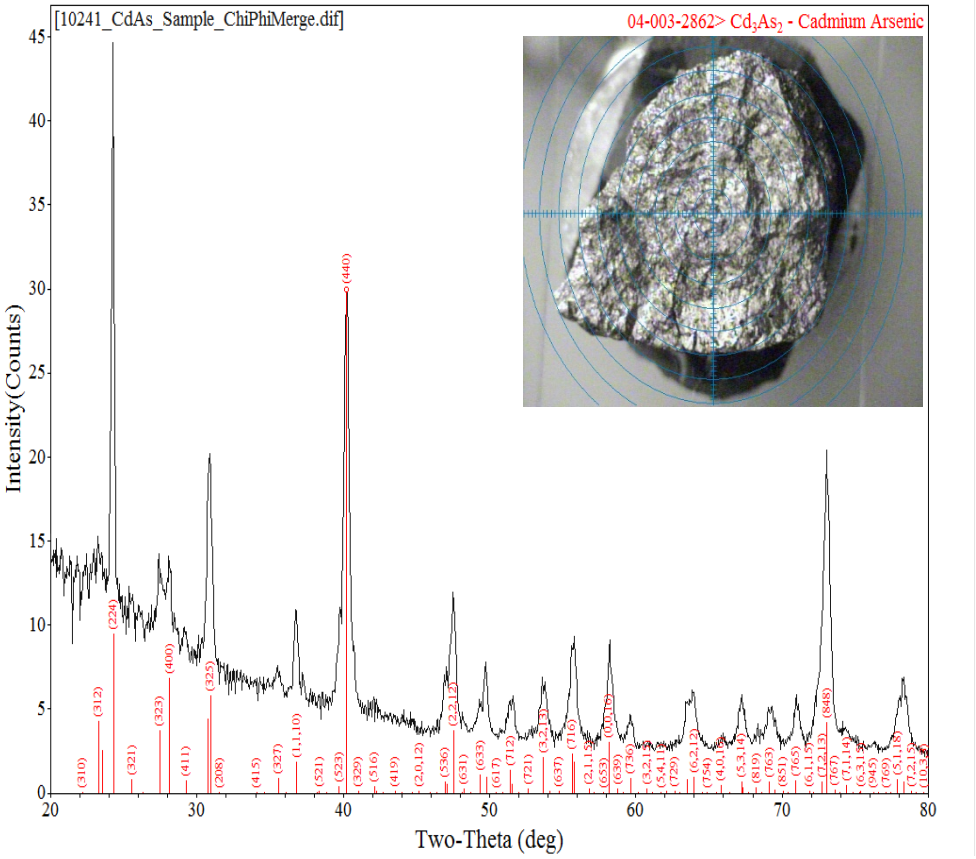

Figure S1: Equivalent powder-diffraction scan of the Cd_3As_2 ingot materials used to fabricate the Al-Cd_3As_2-Al Josephson junctions. All of the observed diffraction maxima correspond with expected reflections for single-phase Cd_3As_2 (plotted as vertical red lines along the bottom edge of the figure). The x-ray diffraction (XRD) data were acquired using a Bruker D8 micro-diffraction system equipped with an area detector, with the ingot scanned in two-theta at each of 14 x 60 sample tilt and rotational orientations. The resulting multidimensional diffraction-data sets were post-processed and merged to derive both the equivalent powder-diffraction scan shown in Fig. S1 and the conventional pole-figure representations shown in Fig. S2. The inset shows a photograph of the ~ 8x10x2 mm^3 ingot as mounted for the XRD analysis.

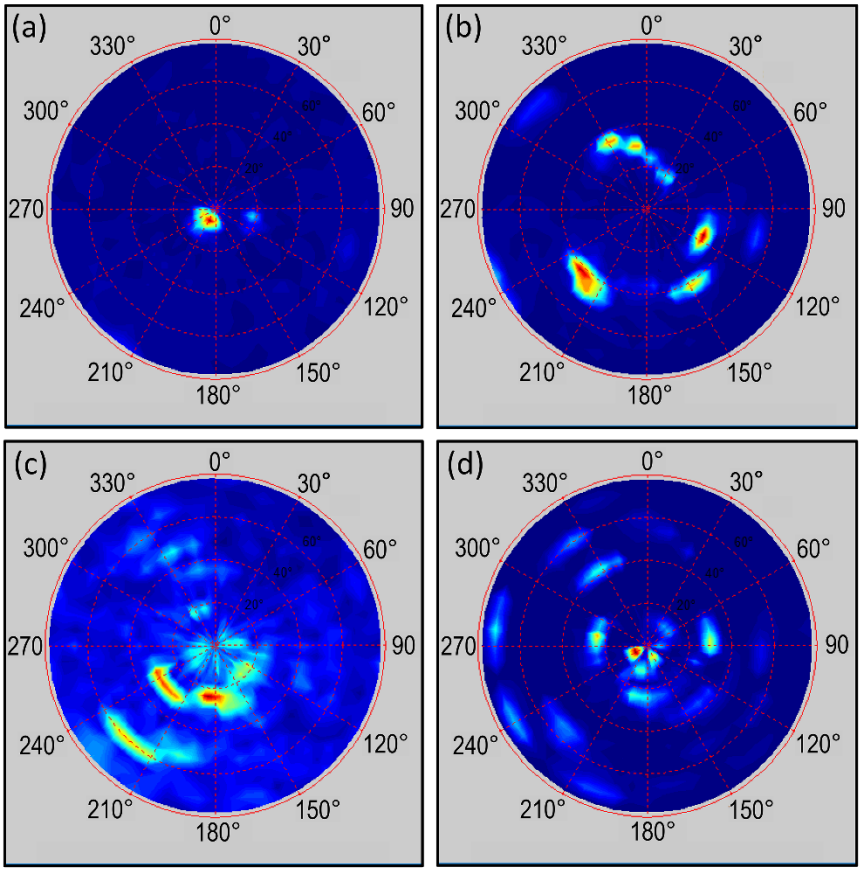

Figure S2: **Equivalent XRD pole figures plotted for selected two-theta angular ranges and corresponding Cd_3As_2 reflections: (a)** 2θ = 24.2-24.45° about (224), **(b)** 2θ = 40-40.5° about (440), **(c)** 2θ = 70.7-71.3° about (765), and **(d)** 2θ = 72.9-73.3° about (848). The plotted azimuthal angle indicates the sample rotation (ϕ), and the plotted radial angle indicates the sample tilt (χ), where χ ranges from 0-78°. Relative diffraction intensities are plotted on a normalized linear scale for each pole figure. The observed pole-figure diffraction maxima are relatively small in number and exhibit a discontinuous and spotty character free of any systematic orientation. These diffraction characteristics indicate that the Cd_3As_2 ingots are comprised of large, randomly oriented polycrystals. The small number of randomly oriented diffracting crystallites explains why the measured peak intensities seen in Fig. S1 do not precisely mirror the relative intensities expected for a random-powder diffraction pattern (shown in red in Fig. S1).

Cd_3As_2 thin flakes preparation and magnetoresistance

Cd_3As_2 thin flakes are obtained from the source ingots by a mechanical method: Two thick, high-purity, polished sapphire wafers are used to capture and crush Cd_3As_2 ingot fragment to form a fine, granular powder. Then, Cd_3As_2 thin flakes are simultaneously created and transferred to a Si/SiO2 carrier substrate by sliding the Si/SiO_2 substrate across the face of one of the sapphire wafers holding the Cd_3As_2 powder. In order to make the Cd_3As_2 flakes as thin as possible, we apply high mechanical pressure to the Si/SiO_2 substrate during the final sliding step. Because high mechanical shearing forces are applied to obtain the nm-scale flakes, minute portions of the sliding SiO_2 layer may locally fracture to become incorporated into the exfoliated Cd_3As_2 flakes (see EDS in Fig. S4). Finally, specific flakes are selected for subsequent device fabrication through visual inspection of the carrier substrate by optical microscopy.

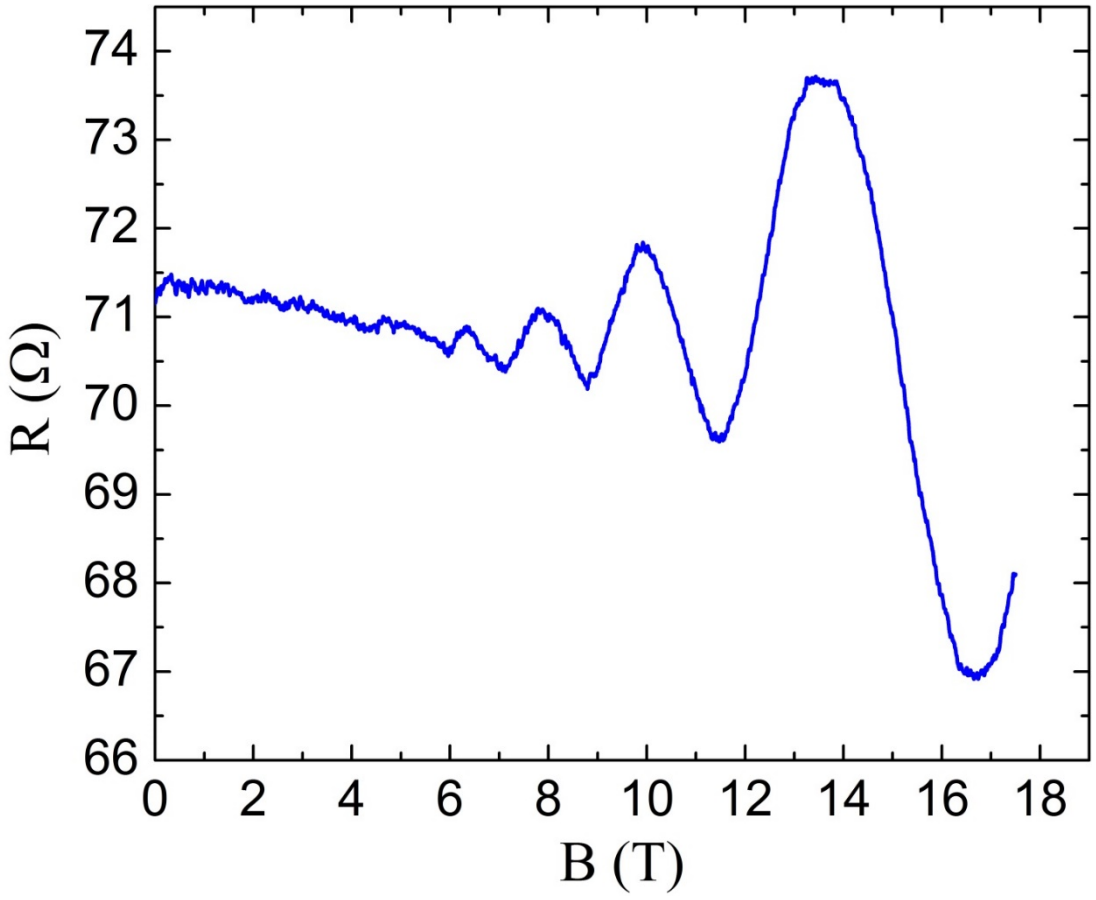

Figure S3. Quantum oscillations in a thin Cd_3As_2 flake with nomal contacts. Magnetoresistance is measured at 0.57 K. Magnetic field is in plane with the Cd_3As_2 flake. Quantum oscillations are observed indicating Cd_3As_2 of a high quality suitable for use in transport studies.

Transmission Electron Microscopy

We prepared a cross-sectional transmission electron microscopy specimen from a Cd_3As_2 device structure using a Focused Ion Beam (FIB) system (FEI Helios Nanolab 660 system, FEI/Thermofisher, Hillsboro, OR). Observations were conducted using an FEI 80-200 Titan Scanning Transmission Electron Microscope (STEM) operated at 200 keV and equipped with a 4-SDD SuperX energy dispersive x-ray spectrometer (EDS). EDS spectra were analyzed using the commercial Bruker Esprit (v 2.1) software package and quantified using library standards provided with the software.

Figure S4(a) presents a bright-field STEM image of the device in cross-section, illustrating the SiO_2 of the underlying oxidized Si wafer, the Cd_3As_2 flake, and the aluminum contact. An EDS map from the indicated region is shown in Figure S4(b). A higher magnification EDS map is shown in Figure S4(c).

The interfaces between the flake and SiO_2 and the Aluminum are sharp and flat. We see no evidence for a significant inter-reaction between the Cd_3As_2 and the Aluminum contact. The EDS spectra collected from within the Cd_3As_2 layer do detect a weak Aluminum signal that would correspond to less than 2 at. %. However, we believe that this low-level signal is likely an artifact resulting from secondary flourescence of the immediately adjacent Al layer.

We also observe some silicon-rich inclusions in the Cd_3As_2 (Figure S4(b)). The origin of these inclusions is unclear. Although they could be present in the original, as grown material, another possibility is that they are incorporated from particles on the wafer as a result of the high shearing forces during the transfer process to the Si/SiO_2 wafer.

Considering only the contributions from the Cd and As signals, quantification of the EDS gives a composition of 59±7 at. % Cd and 41 ± 1 at. % As, which is consistent with the expected composition of 60 at. % Cd and 40 at. % As.

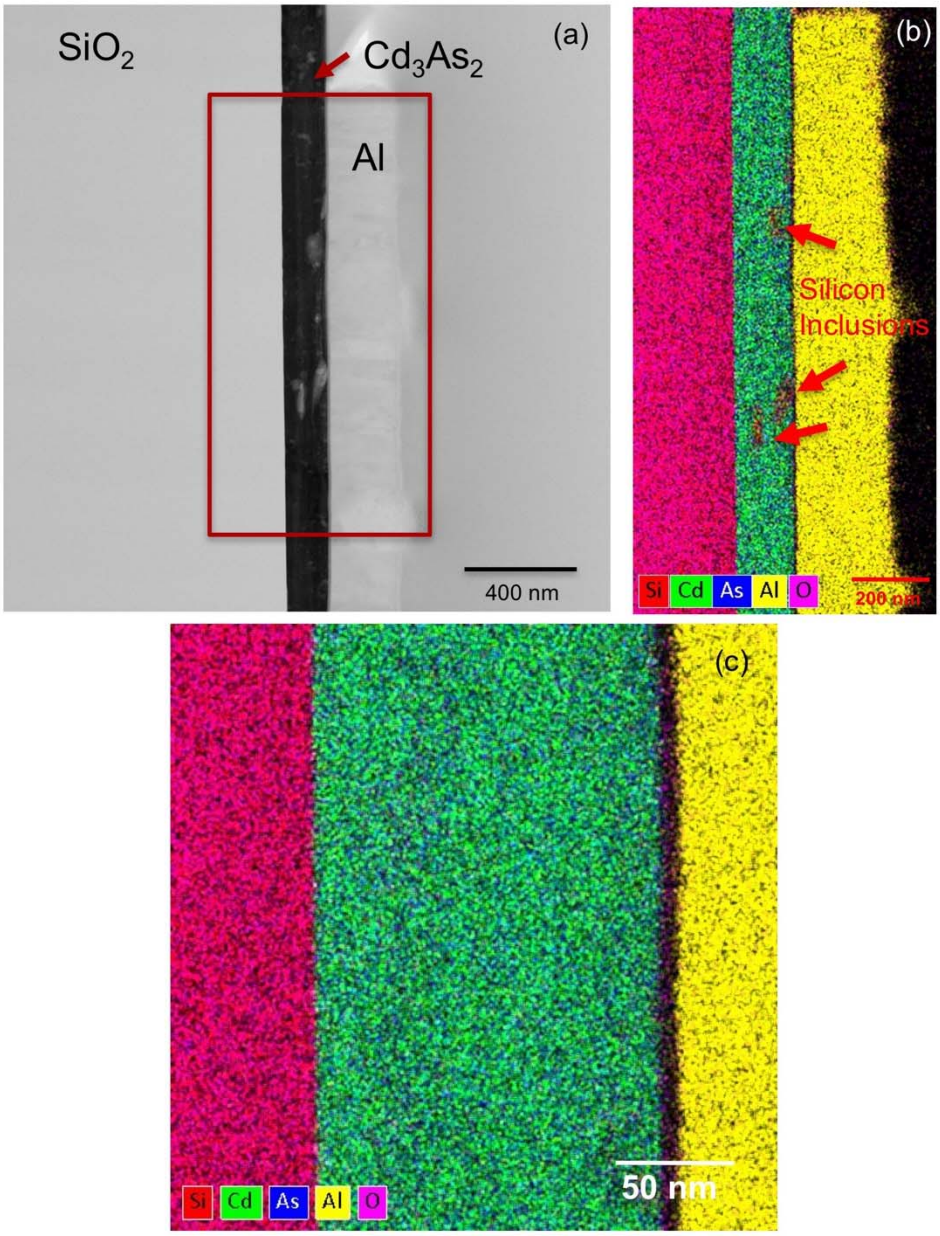

Figure S4: **Scanning transmission electron microscopy (STEM) results.** (a) BF-STEM image of a Cd_3As_2 device structure in cross-section. (b) EDS composite map from the region of (a) marked by the red box. (c) A higher magnification EDS map.

Junction B

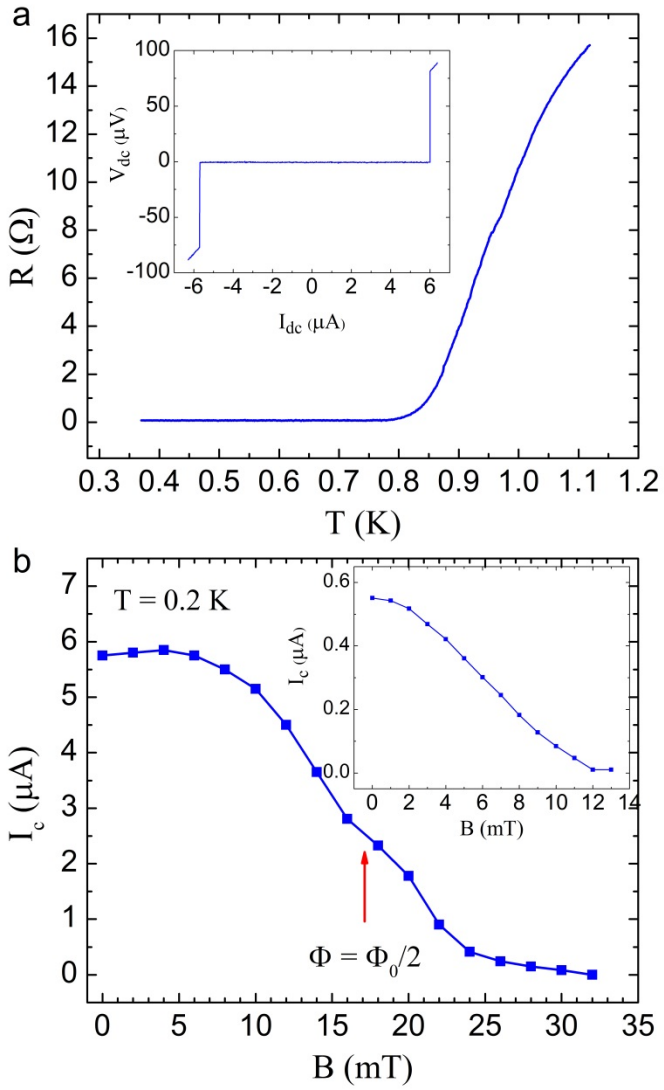

Figure S5. Transport properties of Junction B: (a) The resistance of Junction B is plotted as a function of temperature. The critical temperature is about 0.8 K. Inset shows *I-V* curve measured at 0.2K. A clear supercurrent state is observed. **(b)** Critical current I_c is plotted versus B at 0.2 K. I_c increases with B in the low field regime. A minimum is visible at ~ 17 mT corresponding $\Phi = \Phi_0/2$ indicating π–period supercurrent. Φ_0 is the magnetic flux quantum. Inset shows I_c versus B at 0.7 K. I_c enhancement is suppressed by temperature.

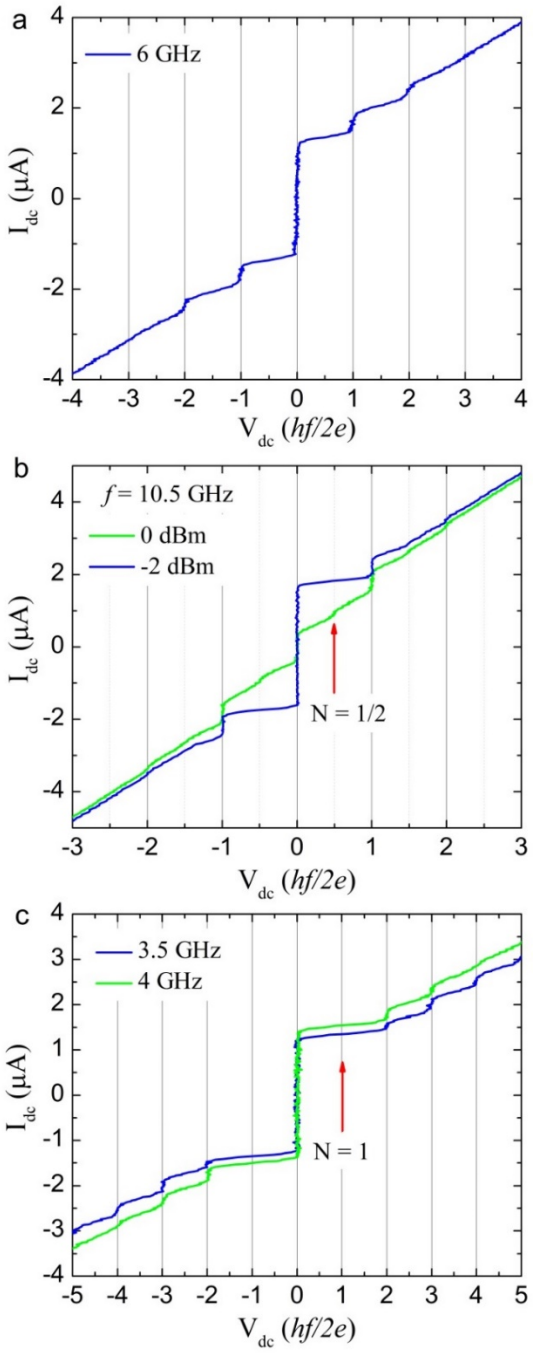

Figure S6. Shapiro steps in Junction B: (a) *I-V* curves measured with microwave irradiation *f* = 6 GHz Integer Shapiro steps are visible at V_{dc} = n*hf/2e*. **(b)** *I-V* curves measured with microwave irradiation *f* = 10.5 GHz. For low irradiation power, Shapiro steps occur at integer numbers (blue trace). With increasing irradiation power, fractional Shapiro steps are observed as marked by the red arrows (green trace). **(c)** *I-V* curves at different frequencies demonstrating 4π-periodic Josephson effect (Step N = 1 is missing).

Theoretical Calculations on Anomalous Shapiro Steps

In addition to integer Shapiro steps, half-integer Shapiro steps also emerge in our experiment. In this section, we analyze the origin of both the integer and half-integer Shapiro steps.

Because of the coexistence of surface-state and bulk-state channels in the Dirac semimetal, our Josephson junction can be viewed effectively as a superconducting quantum interference device (SQUID). Such a device can then be described by a resistively shunted junction model [1] as follows:

$$\begin{aligned} I_j &= \frac{V_j}{R_j} + I_{cj}\sin\phi_j\,, \\ \frac{d\phi_j}{dt} &= \frac{2e}{\hbar}V_j\,, \\ \phi_b - \phi_s &= \frac{2\pi}{\Phi_0}\Phi\,, \#(1) \\ \Phi &= L(I_s - I_b) + \Phi_{\text{ex}} + \Phi_{\text{in}}\,, \\ V &= V_j + L\frac{dI_j}{dt} = V_0 + V_1\cos\omega_f t\,, \end{aligned}$$

where j = b and s stand for the bulk and surface, respectively. In Eqs. (1), I_j, R_j, and I_{cj} denote the current, resistance, and superconducting critical current in the j-channel; V_j and ϕ_j are the voltage and phase difference across the j-channel; Φ_0 is the magnetic flux quantum, L is the self-inductance, Φ_{in} is the intrinsic phase difference between the bulk and surface channels, Φ_{ex} is the phase difference induced by an external magnetic flux if feasible ($\Phi_{\text{ex}} = 0$ in our experiment), and V is the applied voltage.

For simplicity, we choose $R_b = R_s = R$ and $I_{cb} = I_{cs} = I_c$ in our calculation (the conclusion does not change in the more general case) and denote $\tau = 2\pi R I_c t/\Phi_0$, $\beta = LI_c/\Phi_0$, and $i = (I_a + I_b)/I_c$. Thus, Eqs. (1) lead to the following two equations:

$$\begin{aligned} \frac{d\phi_s}{d\tau} + \sin\phi_s + \frac{\phi_s - \phi_b}{4\pi\beta} &= \frac{1}{2}\left[i - \frac{1}{\beta}\left(\frac{\Phi_{\text{ex}}}{\Phi_0} + \frac{\Phi_{\text{in}}}{\Phi_0}\right)\right], \#(2a) \\ \frac{d\phi_b}{d\tau} + \sin\phi_b - \frac{\phi_s - \phi_b}{4\pi\beta} &= \frac{1}{2}\left[i + \frac{1}{\beta}\left(\frac{\Phi_{\text{ex}}}{\Phi_0} + \frac{\Phi_{\text{in}}}{\Phi_0}\right)\right]. \#(2b) \end{aligned}$$

By denoting $\Psi = (\Phi_{\text{ex}}+\Phi_{\text{in}})/\Phi_0$ and expanding Eqs. (2) to the first order in β [2], we obtain the current:

$$I = 2\text{Im}\left[xe^{i\phi_0}\sum_{k=-\infty}^{\infty} J_{-k}(a)e^{i(\omega_0 - k\omega)\tau} + \pi\beta y^2 e^{i2\phi_0}\sum_{k=-\infty}^{\infty} J_{-k}(2a)e^{i(2\omega_0 - k\omega)\tau}\right], \#(3)$$

where $x = \cos\pi\Psi$, $y = \sin\pi\Psi$, $\omega_0 = V_0/RI_c$, $a = 2\pi V_1/\omega_f\Phi_0$, $\omega = \Phi_0\omega_f/2\pi RI_c$, ϕ_0 is an initial constant, and J_k is the k-th order Bessel function.

Therefore, the Shapiro steps emerge at $\omega_0 = k\omega$ and $\omega_0 = k\omega/2$ with k being integers, which respectively produce non-oscillating components in the first and second terms of Eq. (3). For appearance of half-integer steps, the second term needs to be non-zero, i.e., the self-inductance L exists and the phase difference between the two channels is not an integer multiple of 2π. Moreover, the half-integer steps

become prominent when L is large (but still sufficiently small for the consideration of higher order terms in Eq. (3)) and when the phase difference is close to a half integer multiple of 2π. Given $\Phi_{\mathrm{ex}} = 0$ in our experiment, the presence of half-integer Shapiro steps implies that the surface-state and bulk-state channels form a spontaneous 0-π junction (at least close to π).

References:

[1] C. Vanneste, C. C. Chi, W. J. Gallagher, A. W. Kleinsasser, S. I. Raider, and R. L. Sandstrom, *Shapiro steps on current-voltage curves of dc SQUIDs*, J. Appl. Phys. **64**, 242 (1988).

[2] F. Romeo and R. De Luca, *Shapiro steps in symmetric p-SQUID's*, Physica C **421**, 35 (2005).